Methodology for Inkjet Printing Partially Wetting Films

Dan Soltman; Department of Electrical Engineering and Computer Science, University of California; Berkeley, California; Ben Smith; Department of Mechanical Engineering, University of California; Berkeley, California; S.J.S. Morris; Department of Mechanical Engineering, University of California; Berkeley, California; Vivek Subramanian; Department of Electrical Engineering and Computer Science, University of California; Berkeley, California

Abstract

Inkjet printing is widely used as a technique for the fabrication of printed electronic devices. Here we present an analytic treatment of the inkjet printing of two dimensional features with a partially wetting ink. We develop and demonstrate an algorithm for generating variable line spacings that leads to printed features superior to those possible at any fixed spacing. By modeling printed bead shape during the print and by compensating for evaporation, we are able to accurately control a feature's contact angle as it is printed, line-by-line. Finally, we model the maximum corner curvature possible in an equilibrium, partially wetting feature with a positive retreating contact angle and confirm our results with a non-volatile printed system.

Introduction

Solution processing presents a low cost, environmentally friendly alternative to traditional microfabrication techniques. Its additive processing presents an alternative to the slow, costly steps of photolithography and vacuum deposition. Solution processing techniques include roll-to-roll patterning and inkjet printing, the latter being the focus of this work. Researchers have fabricated various microelectronic devices with inkjet printing including transistors, displays, and sensors.[1-3] All of these devices make use of combinations of printed rectilinear shapes. Thus, an understanding of the formation of a rectangle is a logical starting point to optimize the fabrication of arbitrary patterns.

Advancing inkjetted device fabrication requires a better understanding of the behavior of printed fluids on an impermeable substrate. For example, the surface and footprint of inkjetted lines have been studied and optimized.[4, 5] Regarding two dimensional printed films, Tekin et. al. optimized the inkjet printing of polystyrene films.[6] They found that printing several spatially-offset layers at sufficiently low print head velocity leads to more uniform dried films. By choosing a two solvent mixture with differentiated vapor pressures they were able to avoid mass transfer to the film edge, known as the coffee ring effect. This work does not dwell upon such drying effects, but rather is concerned with the shape of beads during and shortly after a print. Kang et. al.[7] used a one dimensional geometric approach to model basic printed film properties including thickness and fluid bulging beyond an intended footprint. In this work, we build upon the approach of Kang et. al. to understand and optimize the shape of patterned beads by examining inkjet-printed patterns under more general conditions including two-dimensional curvature and mass loss.

Experiment

We print our films with a custom-built, drop-on-demand inkjet printer. It has a jetting frequency of 22.3 Hz and a drop volume of 94.8 pL. In the first portion of this work we use an ink consisting of a polymer dissolved in a 1-hexanol (≥99.0%, from Fluka). We chose a polymer commonly used as a dielectric in organic, solution-processed devices, specifically poly-4-vinylphenol (PVP), MW ≈ 8,000 from Sigma Aldrich Co.[1, 8, 9] To prepare our ink, we mix 72 mg of PVP per milliliter of 1-hexanol. We mechanically agitate and then sonicate the solution for ten minutes each, at which point the PVP powder is fully dissolved.

We print onto 5 cm by 7.5 cm rectangles of display-grade Corning 1737 glass. Using a Kruss contact angle measuring system, we measure a quasi-static advancing contact angle (θ_{adv}) of 26.0±1.5° and a receding contact angle (θ_{rec}) of 15.7±1.0°.

We print our films in a raster-scan method, printing in both fast-scan directions as shown schematically in Figure 1. In this work, we printed lines with a 50 μm drop spacing. When building a rectangle, line-by-line, we either keep line spacing constant or use a geometric approach to determine the next line's optimal location as will be discussed later. In this work, we print squares with side lengths ranging from 0.25 mm to 2.0 mm.

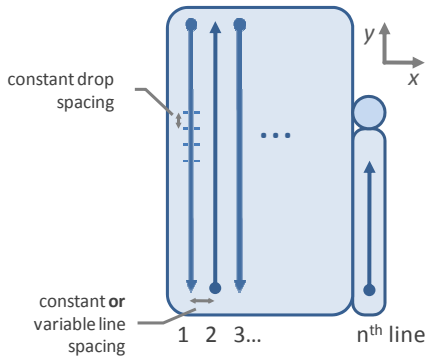

Figure 1. Schematic of raster-scan pattern used to print films as viewed from above.

For the second portion of this work, concerning rounded corners, we print 1-butyl-3-methylimidazolium tetrafluoroborate ('BMT') obtained from Sigma-Aldrich Co, chosen for its low vapor pressure and partial wetting. We again use Corning 1737 glass substrates, now roughened by hand using $1\mu m$ grade lapping paste to created a controlled contact angle hysteresis. We clean the substrate by sonicating and then rinsing in order with deionized water, acetone and isopropanol, and drying after each rinse with a nitrogen gas gun. We measure a quasi-static advancing contact

angle (θ_{adv}) of 26.9°±0.5° and a receding contact angle (θ_{rec}) of 5.1°±3.6°.

Raster scan printing

A simple approach to printing a two-dimensional film, such as a square, is to print the feature by a raster-scan method, as shown in Figure 1, with a constant, identical spacing in both x and y directions. Figure 2 shows 2.0 mm to 0.25 mm dried squares at their respective best-case constant drop spacing, showing minimal bulging and/or separation. The border of dried beads in this and later figures is the most important feature in understanding the patterning of two dimensional shapes. Each bead also shows a uniform interior and a "coffee ring" transfer of solute to its border. The precise nature of the coffee ring is a function of local bead shape and evaporation but is irrelevant to this work concerned with the patterning of two-dimensional beads during a print. Recall that co-solvents can prevent this coffee ring deposit, but in this work we did not wish to further complicate our system by using an ink whose contact angle varies with local evaporation.

Beginning with the 2.0 mm squares, we see that there is substantial bulging on the left-hand side of the 20 µm-spaced square where printing began. Increasing the drop spacing to 30 µm reduces this bulge, but the right-hand side is now separated into small, isolated beads. The 1.0 mm and 0.5 mm squares show a similar transition in planform, from left-hand side bulging to right-hand side separation, although at larger spacings as the length scale shrinks. Finally, the smallest 0.25mm squares show a large amount of rounding on all sides, deviating the most from a square footprint. Thus, we see that a fixed spacing printing method is not viable for systems with a narrow contact angle hysteresis.

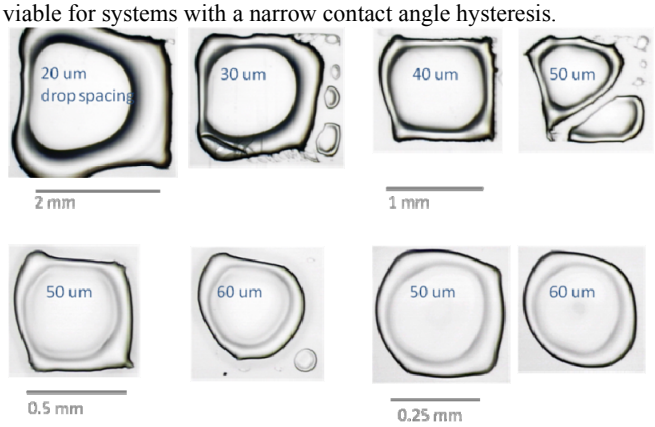

Figure 2. Squares printed at constant horizontal and vertical drop spacing as noted. Side lengths (clockwise from top left): 2mm, 1mm, 0.25mm, 0.5mm.

Model for the droplet shape

A concise explanation for the deviations from squareness seen in Figure 2 can be made by examining a bead's maximum contact angle as it is printed, line by line. In order to estimate a printed bead's contact angle, we require a mathematical model for its surface. The contact lines of the bead are assumed to be pinned to the edges of a 2a by 2b rectangle as shown in Figure 3. We use a small slope approximation to find an analytic approximation for the surface of our printed bead because of the small advancing contact angle. We further assume that the bead's moving contact line is sufficiently slow that it advances at the quasi-static θ_{adv}.

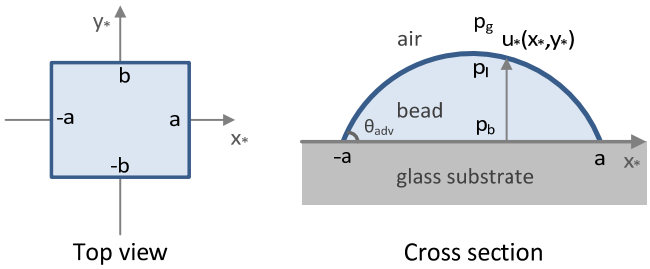

Figure 3. Top view and cross section of bead surface.

The Young-Laplace equation and hydrostatic pressure determine the surface of our quasi-static rectangular bead, and here we develop an analytic solution. Because our ink-substrate system has a low contact angle, with errors vanishing as the square of the slope, we may approximate the curvature of the surface $z = u_*(x_*, y_*)$ by $\nabla^2 u_*$. The pressure at any point at the bottom of the bead, p_b in Figure 3, is the sum of the ambient, Young Laplace, and hydrostatic pressures as given in Eq 1 below.

$$p_b = p_g + \rho g\, u_*(x_*, y_*) - \gamma \nabla^2 u_*(x_*, y_*) \quad (1)$$

Assuming an equilibrium bead with constant base pressure, the resulting boundary value problem for $|x| < 1$ and $|y| < \beta$ is as follows, after appropriate non-dimensionalization. We define the bead's Bond number as $Bo \equiv \rho g a^2/\gamma$.

$$\nabla^2 u - Bo\, u = -1 \quad (2a)$$

$$u(\pm 1, y) = 0 \quad (2b)$$

$$u(x, \pm\beta) = 0 \quad (2c)$$

$$\int_{-1}^{1} dx \int_{-\beta}^{\beta} dy\, u(x,y) = V_{bead} \quad (2d)$$

Expanding both sides of Eq. 2a in a double Fourier series, we obtain the following solution:

$$u(x,y) = \frac{-64}{\pi^4} \sum_{m=0}^{\infty} \sum_{n=0}^{\infty} \frac{(-1)^{(m+n+1)}}{(2m+1)(2n+1)} \cdot \frac{\cos\left((2m+1)\frac{\pi}{2}x\right)\cos\left((2n+1)\frac{\pi y}{2\beta}\right)}{\left[(2m+1)^2 + \left(\frac{2n+1}{\beta}\right)^2 + \frac{4}{\pi^2}Bo\right]} \quad (3)$$

Figure 4 shows the maximum bead contact angle, θ_{max}, calculated from Eq. 3 as a 2mm square is printed, line by line, which we find useful in explaining the printing behaviors in Figure 2. (The maximum contact angle is found at the center of the longest side of the rectangular bead.) Each additional line introduces an additional ink volume of the drop volume times length divided by drop spacing. In Figure 4, we see that the early bead's maximum contact angle begins at a large value, well above the advancing contact angle, and decreases monotonically as each new line is added. The bulging on the left side of squares in Figure 2 is due to the initial region of lines printed with the bead's θ_{max} above θ_{adv}. As more lines are printed, the bead then goes through a régime where additional lines maintain θ_{max} between the advancing and receding contact angles. With the printing of sufficient lines, θ_{max} may fall below θ_{rec} at which point the bead's edge will retreat until its maximum contact angle rises to θ_{rec}. Because the right side is printed most recently, its contact line has seen the least

evaporation and retreats most readily. When the edge retreats, new lines may no longer reach the principal bead and separation may occur, as seen in the right side of many Figure 2 squares. Unfortunate beads, like the 0.5 mm square printed at a 50 µm spacing, may experience both left-hand side bulging and right-hand side separation.

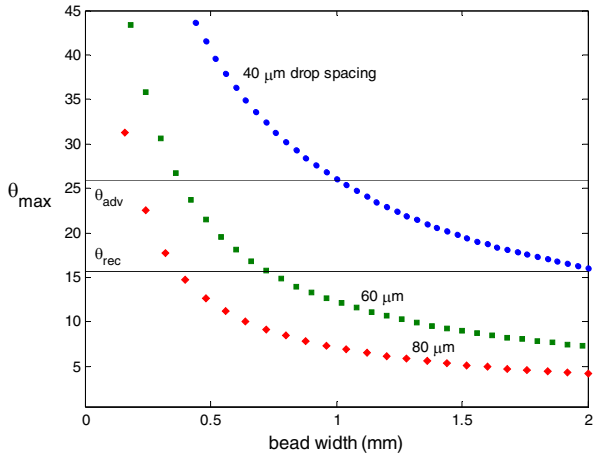

Figure 4. Maximum bead contact angle calculated from Eq. 3 versus bead width for specified constant drop spacings (same in both fast and slow print directions) for a 2 mm square. Each point represents an additional printed line.

Variable line spacing

As was demonstrated and explained in section 4, a rectangular bead's maximum contact angle, θ_{max}, will vary with each additional line if a constant line spacing is used. This leads to undesirable bulging and separation when the contact angle falls outside of the range between θ_{rec} and θ_{adv}. A practical solution to this problem is to print each additional line at a spacing such that the bead's maximum contact angle remains constant as the feature is created. Figure 5a outlines the algorithm we implemented for generating such optimal spacings for a printed rectangle.

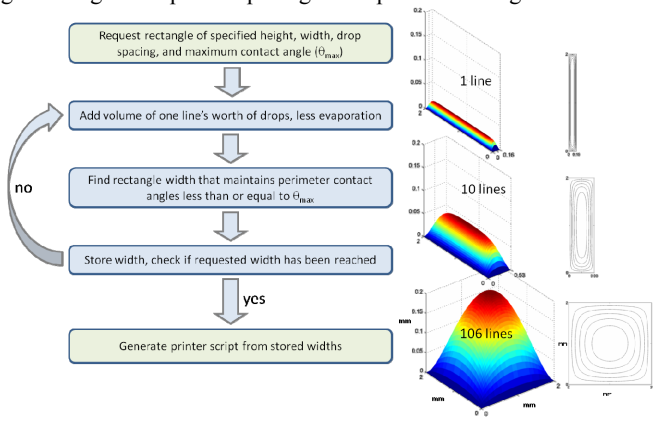

a) Spacing-generating algorithm

b) Surface and contour plots of square in progress

Figure 5. a) Spacing-generating algorithm for printing a rectangle, b) surface and contour plots of a 2mm square in progress. (Each contour line represents one sixth of height.)

In order to print a rectangle of specified width and height while maintaining a specified θ_{max}, we begin by finding the width of a single line's worth of drops that will have the requested θ_{max} according to Eq. 3. The volume used in this calculation is the drop volume times the number of drops required to complete the fast-print line less evaporation that occurred while that line was printed. For expediency, we use an empirically-based fit for evaporative loss at a specified number of drops. After finding the width of this first line, we store this number and increment the bead volume by the volume of another lines worth of drop, less evaporation. We continue repeating this width calculation with increasing volume until the entire rectangle has been spanned. A final script converts this list of widths to a jetting script for our drop-on-demand printer.

For squarest squares, we set the printing θ_{max} at θ_{adv}. As the contact angle is largest at a side's center and decreases towards the corners, this maximizes the length of contact line between θ_{max} and θ_{rec} without risking bulging. With θ_{max} set at θ_{adv} and other input parameters set to the values from the experimental section, we were able to run our algorithm for a variety of rectangles.

Using our algorithm to find optimal line spacings and generate printer files, we printed an array of squares sized 0.5 mm, 1 mm, and 2 mm. We show the resultant dried patterns in Figure 6. Without evaporation compensation all three size scales separate and retreat from their designed footprint as seen in the leftmost column. When additional volume is added to match evaporation, all three beads print intact. The largest square remains closest to its desired footprint while the smaller ones have progressively worse corner curvature where the bead has withdrawn from the corner towards its center.

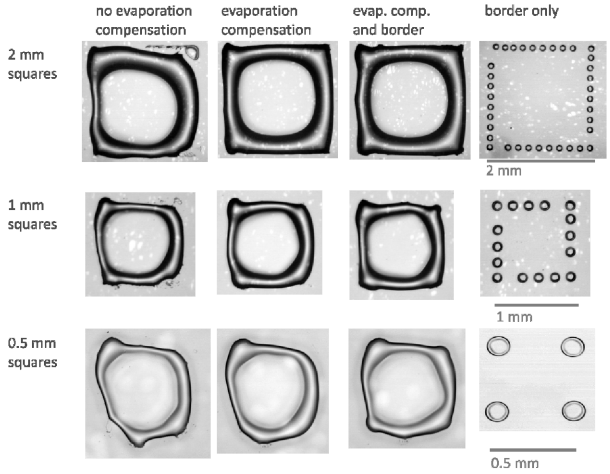

Figure 6. Squares printed using algorithm-generated spacings with evaporation compensation and pre-printed border as noted.

Comparing the four corners of each smaller square, we see that the top left corner is the furthest from the drop center. Apparently, this corner is the most pinned. Our prints begin at the corner and proceed down, indicating that here the timescale for contact line pinning due to drying is on the same order as that of the print time. By deliberately pre-printing and drying a feature's border, we were able to improve its footprint. We pre-printed isolated drop borders and allowed them to dry before returning to print the square beads themselves, as seen on the right side of

Figure 6. The third column of this figure shows that pre-printed edges lead to enhanced squares. The pre-dried edges have a greater contact angle hysteresis than when printing on the clean substrate and thus permit a planform that is less circular and has sharper corners.

Corners

Differentiating Eq. 3 reveals that the contact angle falls to zero as the contact line approaches a perfectly sharp corner. We hypothesize that a drop will be stable if the contact angle θ around the entire contact line remains within the limiting values of advancing and receding contact angles, or $\theta_R \leq \theta \leq \theta_A$. We also assume that for a drop pinned on particular boundary, the maximum contact angle will be the advancing contact angle and the minimum contact angle will be the receding contact angle. Therefore for a given drop we are most interested in the maximum and minimum contact angle around a drop boundary, θ_{max} and θ_{min}.

Using Eq. 2a, we built a finite element model and applied it to square-ish beads with circular arcs fitted into the corners. Some examples showing how the contact angle varies around the boundary of squares with various amounts of corner rounding are shown in Figure 7. The contact angle maxima θ_{max}, of each square occur half way along the edge, and the minima θ_{min}, occur at the corners. There are two limiting cases; when $r = 0$ and when $r = 0.5$. When $r = 0.5$, the drop takes the shape of a circular drop with constant perimeter contact angle. When $r = 0$, the perimeter contact angle falling to zero in the bead's corners. In Figure 7, we computed the contact angles around boundaries with $r = 0.15, 0.3, 0.5$ with our numerical model.

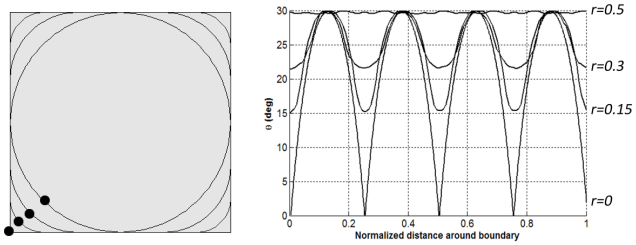

Figure 7. Contact angle around drop contact line for various shape drops. The plot follows the boundary counter-clockwise starting at the dots.

Figure 8 show a representative square bead printed with the BMT-polished glass system with its constant, time-invariant contact angle hysteresis. The line spacings used to generate the bead were calculated using the spacing-generating algorithm outlined in the previous section. We see that the corners do retreat approximately as circular arcs, as predicted above.

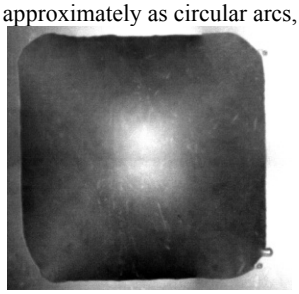

Figure 8. Rounded 2mm BMT square bead

Figure 9 shows extracted experimental results plotted against numerical predictions for a broad range of bead sizes. For the experimental data, r^* was taken as the average of the four corners. A key prediction of the numerical model is that r^* is independent of drop size. Figure 9 shows that over nearly one order of magnitude in edge length there is no significant variation in r^*. As the dimensional edge length a is decreased, r^* increases. This behavior is likely due to the corner rounding becoming limited by the jetted drop size. We expect the jetted drop size to more strongly influence the corner rounding as the overall size of the drop is decreased. This seems reasonable as the smallest drop ($a = 125$ μm) was printed using only four jetted drops.

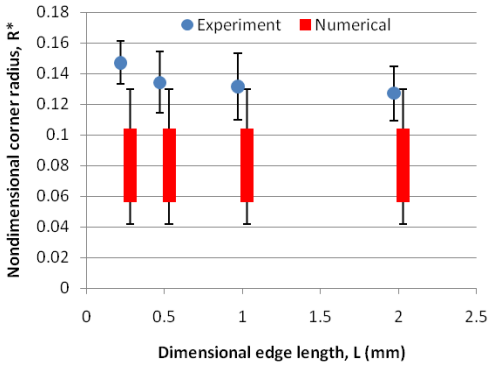

Figure 9. Corner radius r plotted against dimensional edge length, numerical and experimental results both plotted.*

Conclusion

We have demonstrated and then overcome difficulties in inkjet printing a patterned, two dimensional film with narrow contact angle hysteresis. A fixed line spacing approach leads to a varying bead contact angle as new lines are printed, creating first bulging and later bead separation. We developed and implemented an algorithm to find the spacing that will maintain a bead's contact angle as it is printed by appropriately adjusting line spacing. We found that it is necessary to compensate for evaporation as the print progresses to maintain the optimal contact angle. Using our spacing generator with evaporative compensation, we demonstrated printed squares with footprints superior to those printed at fixed spacing over a range of length scales. By seeding a feature's edge with isolated dried drops, we were able to further improve a feature's footprint. However, pre-printing a feature's border introduces a manufacturing cost akin to the printing of an additional layer. We must print the border, wait for the isolated border drops to dry (on the timescale of milliseconds), and then proceed with the printing of the feature.

Finally, we utilized a non-volatile ink to demonstrate the receding contact angle imposed limit on corner sharpness in rectangular beads. Our experimental results are in agreement with simulation.

Acknowledgment.

The Semiconductor Research Corporation, Applied Materials, and the World Class University Program at Sunchon National University, South Korea supported this work.

Author Biography

Dan Soltman is a graduate student in the Organic Electronics group at the University of California, Berkeley. His research focuses on hydrodynamic concerns in printed electronics. He earned a bachelor's degree in electrical engineering at Brown University in 2004 and a master's degree in electrical engineering at UC Berkeley in 2007.

References

[1] V. Subramanian, *et al.*, "Printed organic transistors for ultra-low-cost RFID applications," *Ieee Transactions on Components and Packaging Technologies,* vol. 28, pp. 742-747, Dec 2005.

[2] S. C. Chang, *et al.*, "Dual-color polymer light-emitting pixels processed by hybrid inkjet printing," *Applied Physics Letters,* vol. 73, pp. 2561-2563, Nov 1998.

[3] M. F. Mabrook, *et al.*, "Inkjet-printed polypyrrole thin films for vapour sensing," *Sensors and Actuators B-Chemical,* vol. 115, pp. 547-551, May 2006.

[4] P. C. Duineveld, "The stability of ink-jet printed lines of liquid with zero receding contact angle on a homogeneous substrate," *Journal of Fluid Mechanics,* vol. 477, pp. 175-200, Feb 2003.

[5] D. Soltman and V. Subramanian, "Inkjet-printed line morphologies and temperature control of the coffee ring effect," *Langmuir,* vol. 24, pp. 2224-2231, Mar 2008.

[6] E. Tekin, *et al.*, "Ink-jet printing of polymers - from single dots to thin film libraries," *Journal of Materials Chemistry,* vol. 14, pp. 2627-2632, 2004.

[7] H. Kang, *et al.*, "Hydrostatic Optimization of Inkjet-Printed Films," *Langmuir,* 2010.

[8] G. W. Kang, *et al.*, "The electrical characteristics of pentacene-based organic field-effect transistors with polymer gate insulators," *Current Applied Physics,* vol. 5, pp. 297-301, May 2005.

[9] T. Makela, *et al.*, "Utilizing roll-to-roll techniques for manufacturing source-drain electrodes for all-polymer transistors," *Synthetic Metals,* vol. 153, pp. 285-288, Sep 2005.